JHEP|Reports

PERSoN4: A multiparametric ultrasound model to improve CEUS LI-RADS for HCC

Authors

Giorgio Esposto, Paolo Santini, Linda Galasso, …, Antonio Gasbarrini, Fabio Piscaglia, Maria Assunta Zocco‡

Correspondence

mariaassunta.zocco@unicatt.it (M.A. Zocco).

Graphical abstract

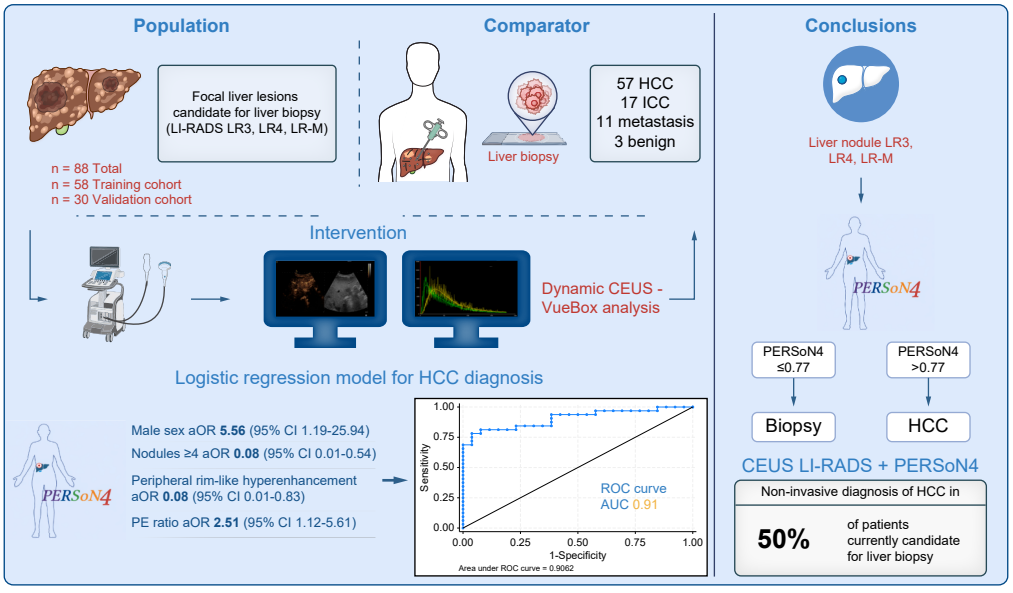

Highlights:

- D-CEUS provides useful non-invasive diagnostic information for malignant or potentially malignant liver nodules in at-risk patients.
- The PERSoN4 model could improve the performance of CEUS LI-RADS criteria for non-invasive diagnosis of HCC.
- PERSoN4 score >0.7729 showed 68.8% sensitivity and 100% specificity, with a PPV of 100.0% and moderate diagnostic accuracy (AUC 0.84).
- This model may enable non-invasive HCC diagnosis in ∼50% of patients currently considered for liver biopsy.

Impact and implications:

Accurate non-invasive diagnosis of HCC remains challenging in patients with atypical vascular patterns on CEUS, providing the scientific rationale for developing a multiparametric D-CEUS-based risk model that integrates quantitative perfusion analysis with clinical and imaging features. Our findings suggest that the PERSoN4 model could meaningfully enhance the diagnostic performance of CEUS LI-RADS, particularly by identifying a subset of patients in whom HCC can be diagnosed with very high specificity and PPV, which is relevant for hepatologists, radiologists, and multidisciplinary tumor boards managing indeterminate nodules. This approach could reduce the need for liver biopsy in nearly half of currently eligible patients, streamlining diagnostic pathways and potentially lowering procedure-related risks and costs. However, given the moderate sensitivity and the limited sample size, further large-scale external validation is essential before widespread clinical implementation.

https://doi.org/10.1016/j.jhepr.2026.101823

Research article

JHEP|Reports

PERSoN4: A multiparametric ultrasound model to improve CEUS LI-RADS for HCC

Giorgio Esposto[1,†], **Paolo Santini**[2,†], Linda Galasso[1], Maria Elena Ainora[1], Alice Giamperoli[3], Lucia Cerrito[1], Raffaele Borriello[1], Irene Mignini[1], Matteo Garcovich[1], Mattia Paratore[1], Laura Riccardi[1], Maurizio Pompili[1], Francesca Romana Ponziani[1], Antonio Gasbarrini[1], Fabio Piscaglia[3,‡], Maria Assunta Zocco[1,‡,*]

JHEP Reports **2026**. vol. 8 | 1–11

Background & Aims: Dynamic contrast-enhanced ultrasound (D-CEUS) could be a valuable tool for the non-invasive diagnosis of hepatocellular carcinoma (HCC) with atypical vascular imaging features.

Methods: Between January 2021 and November 2023, consecutive patients with chronic liver disease and liver nodules who were candidates for liver biopsy were enrolled in this cohort study. CEUS was performed in all patients before biopsy and categorized according to the CEUS Liver Imaging Reporting and Data System (LI-RADS). Clips were examined using VueBox® software. Clinical and ultrasound parameters were compared among the different histological entities, analyzed with univariable analysis, and incorporated into a logistic regression model for HCC diagnosis. The diagnostic accuracy of the identified model was evaluated by receiver operating characteristic (ROC) curve and relative AUC. The model was then tested on a validation cohort comprising consecutive patients from two centers.

Results: A total of 88 patients (57 with HCC, 17 with intrahepatic cholangiocarcinoma, 11 with liver metastases, and three with benign lesions) were enrolled. Statistically significant differences between patients with and without HCC in the training cohort were incorporated in an optimal logistic regression model that included the following predictive variables: sex, number of nodules ≥4, peripheral rim-like hyperenhancement, and peak enhancement (PE) ratio (PE–rim-like enhancement–Sex–Nodules≥4; PERSoN4). The model displayed high accuracy (AUC 0.91) for the diagnosis of HCC. In the validation cohort, the model showed a sensitivity of 48.8% and a specificity of 100.0%, with a positive predictive value (PPV) of 100.0%, maintaining good diagnostic accuracy (AUC of 0.74).

Conclusions: PERSoN4 could improve the performance of CEUS LI-RADS criteria, possibly leading to a non-invasive diagnosis of HCC in nearly 50% of patients currently referred for liver biopsy. However, this model requires further external validation before entering clinical practice.

Introduction

Unlike cancers arising in most other organs, for which histological confirmation is always required to plan treatment, imaging has a major role in the diagnosis of hepatocellular carcinoma (HCC) in high-risk patients.[1] Conventional ultrasound (US) is the preferred surveillance tool for focal liver lesions (FLLs) because of its safety, convenience, and simplicity.[2,3] However, once a lesion is detected, further characterization with contrast imaging is required. Although HCC represents 60–75% of liver nodules >10 mm in patients at risk, regenerative nodules with various degrees of dysplasia also need to be considered and other malignancies can also occur, such as intrahepatic cholangiocellular carcinoma (ICC) or metastasis of extrahepatic cancers. With the ability to assess lesions perfusion in real time, contrast-enhanced ultrasound (CEUS) is among the accepted radiological methods used to characterize FLLs in patients at risk of HCC according to several international guidelines and recommendations.[4–6]

To standardize image interpretation and improve the diagnostic accuracy of suspected HCC, the American College of Radiology (ACR) released the CEUS Liver Imaging Reporting and Data System (LI-RADS), which is now widely used as a diagnostic system for patients at risk of HCC and endorsed by the several international scientific societies.[7–9]

Based on primary features, such as the diameter of the FLL, arterial phase enhancement, and washout occurrence and pattern, the CEUS-LI RADS algorithm evaluates the increasing probability of HCC from LR-1 to LR-5 and provides a LR-M class that includes lesions probably or definitely malignant, but not specific for HCC and, thus, of undefined cellular origin.

* Corresponding author. Address: Fondazione Policlinico Universitario 'A. Gemelli' IRCCS – Università Cattolica del Sacro Cuore – Rome, Largo A. Gemelli, 8, 00168, Rome, Italy. Tel.: +39 06 3015 6018; fax: +39-06 3015 7232.
E-mail address: mariaassunta.zocco@unicatt.it (M.A. Zocco).
† These authors contributed equally.
‡ These authors contributed equally
https://doi.org/10.1016/j.jhepr.2026.101823

Different studies demonstrated that category LR-5 has high specificity in predicting HCC, with a positive predictive value (PPV) of nearly 100%, and this is why a diagnosis of HCC can be confidently achieved with contrast imaging, whereas other patterns would require a histological confirmation, whenever a definitive diagnosis is needed.[10,11]

The working group that designed the criteria made choices that focused on specificity over sensitivity, struggling to achieve the highest PPV for HCC, to limit the risk of false diagnoses in patients with a categorization of LR-5. As a consequence, it is not surprising that validation studies that confirmed the extremely good PPV[11,12] also reported a relatively low sensitivity (44.8–64.2%) and, therefore, a suboptimal global accuracy (60.4–70.8%), given that a significant proportion of HCC still fall within the LR-M, LR-3, and LR-4 categories.[6,13]

Although liver biopsy might appear to be a straightforward procedure and could theoretically clarify lesions not meeting LR-5 criteria, it is frequently technically unfeasible or associated with an unacceptably high risk of complications. The target nodule might be difficult to access or located in high-risk areas (*e.g.* subcapsular or partially exophytic lesions), and patients can present with thrombocytopenia, impaired coagulation, or ascites along the anticipated needle track. Furthermore, some patients might be unable to cooperate or might refuse to undergo such an invasive procedure.

All these considerations suggested the need to improve the diagnostic efficiency of standard CEUS criteria. Some researchers proposed a redefinition of the classification conditions by adjusting the criteria for LR-M and LR-5.[14–16] Ding *et al.* reported that reducing early washout time from 60 to 45 s for LR-M could increase the specificity for differentiating HCC from non-HCC malignancies.[15] Zeng *et al.* found that the sensitivity for HCC was increased by regrouping LR-M categories without marked washout in 3 min to LR-5 lesions.[16]

However, the modification of criteria for the differential diagnosis between HCC and non-HCC malignancies remains problematic, given that any increase in HCC detection sensitivity that associates with a decrease in diagnostic specificity for HCC could be detrimental for the clinical practice. Therefore, attempts have been made to improve the non-invasive diagnostic algorithms and objectivity in the assessment of contrast enhancement behavior. Of note, dynamic CEUS (D-CEUS), an imaging method that allows quantitative evaluation of lesions microvasculature, has been introduced.[17] Several studies have shown good diagnostic accuracy, sensitivity, and specificity of D-CEUS in the characterization of FLLs.[18,19]

To our knowledge, few studies have focused on the role of D-CEUS in the classification of malignant liver lesions in patients with liver disease at risk for HCC,[20,21] in particular addressing the issue of the LI-RADS classes, which are now the categorization tools recommended by both AASLD and EASL guidelines.[22,23]

We hypothesized that D-CEUS could provide useful information for a non-invasive diagnosis of malignant and probably malignant liver nodules not definitively classified according to standard CEUS LI-RADS criteria, which at present would mandatorily require biopsy. Therefore, we evaluated the usefulness of incorporating D-CEUS into the diagnostic algorithm for HCC. The primary objective of the study was the identification of a risk prediction model (RPM) for HCC diagnosis in patients with chronic liver diseases and FLLs considered for liver biopsy as a result of inconclusive radiological findings. Our secondary objective was the identification of D-CEUS parameters associated with HCC diagnosis in the same population.

Patients and methods

Between January 2021 and November 2023, all consecutive patients with FLLs at risk for HCC referred to the digestive disease center of the University Hospital 'Agostino Gemelli' (Rome) for biopsy of the liver lesion were evaluated for enrollment.

Inclusion criteria were as follows: age older than 18 years, high-risk factors for HCC according to the ACR CEUS LI-RADS criteria v2017[7] (*i.e.* liver cirrhosis and chronic HBV infection); computed tomography (CT) and magnetic resonance imaging (MRI) inconclusive for diagnosis; FLL visible on conventional US; inconclusive CEUS LI-RADS class (*i.e.* LI-RADS LR3, LR4, and LR-M) and histological diagnosis provided by liver biopsy. Therefore, we included only patients at high risk of HCC but requiring biopsy for definitive diagnosis.

Exclusion criteria were as follows: a history of previous treatment of the target nodule or a history of HCC and a CEUS LI-RADS or CT or MRI LR5 pattern. In fact, in case of LR-5, pattern nodules would be directly considered conclusive for HCC without further investigation. Other exclusion criteria were cirrhosis caused by vascular disorders, hypersensitivity to the US contrast agent (sulfur hexafluoride, Sonovue®), incomplete D-CEUS data, and poor US image quality.

As a validation cohort, we enrolled a group of patients, with similar characteristics and with a histological diagnosis, collected from archives of the IRCCS Policlinico Universitario Agostino Gemelli (Rome) and IRCCS Azienda Ospedaliera-Universitaria di Bologna.

Study protocol

This was a cohort study including patients with chronic liver disease and FLLs conducted in two Italian university hospitals serving as tertiary referral centres for the diagnosis and treatment of liver diseases. The study protocol was approved by the University Hospital 'Agostino Gemelli' IRCCS Institutional Review Board (identification number: 2824) and registered at clinicaltrials.gov (NCT05977764). All the patients enrolled in the training cohort provided written informed consent.

Histopathological analysis served as the reference standard for the final diagnosis, given that it represents the gold standard for the diagnosis of HCC, particularly when imaging findings are inconclusive. Histological examination was carried out on samples obtained by US-guided biopsy performed within 30 days and usually on the same day of CEUS examination.

Baseline demographic, clinical, and laboratory data were recorded. Laboratory tests included confirmation of chronic liver diseases etiologies, alpha-fetoprotein (AFP) levels, and carcinoembryonic antigen (CA) 19-9 levels, whenever available. Liver cirrhosis was diagnosed by histopathological analysis or imaging methods.[24]

Multiparametric US examination

US studies were performed by two experienced physicians (MEA, with 13 years of experience in liver imaging and FP with 30 years of experience in liver imaging) with Aixplorer Mach 30 (SuperSonic Imagine, Aix-en-Provence, France) equipped with

a wideband C6-1 convex probe (frequency range, 1.0–6.0 MHz) and Esaote MyLab X9 equipped with a wideband C8-1 convex probe (frequency range, 1.0–8.0 MHz).

After a fasting status of at least 6 h, US examination was performed in three phases. The liver was first scanned with conventional US to identify lesions and evaluate basal US features. In cases of multiple lesions in the same patient, only the lesion scheduled for biopsy was considered eligible.

Subsequently, 2D shear wave elastography (2D-SWE) was performed with the same equipment. Measurements were obtained with the patient in a supine position and suspended normal breathing with the right arm raised over the head. The shear-wave measurement box was positioned on the liver lesion to obtain an appropriate SWE map. In the case of very large lesions, we placed the region of interest (ROI) in the most representative part of the FLL. Margins and central necrosis in larger lesions were spared. Elasticity values were displayed in a color-coded 2D image of tissue stiffness in box form over a conventional B-mode image. We considered reliable only those cases with a stability index (SI) of at least 90% when using the Aixplorer Mach 30. The median value of at least three successful measurements was considered for analysis and was expressed in kPa. An IQR to the median ratio (IQR/M) <30% was used as a reliability criterion.

Finally, CEUS with SonoVue® (Bracco, Milan, Italy) was carried out according to European Federation for Ultrasound in Medicine and Biology (EFSUMB) guidelines,[7] almost invariably using a 2.4-ml amount of agent. Signal enhancement of the target lesion and surrounding liver parenchyma were observed in real time and a dynamic sequence covering the first 3 min was recorded continuously on a hard disk for patients in the training group and exported as Digital Imaging and Communications in Medicine (DICOM) for further analysis. In case of multiple FLLs, CEUS was performed on the largest lesion among those that were technically accessible for percutaneous liver biopsy. This approach was adopted to ensure consistency between imaging assessment and histopathological sampling, as well as to maximize diagnostic reliability.

Image analysis

B-mode US and CEUS images were reviewed by two operators with more than 10 years of experience in liver US imaging (LG and MEA) to both clinical and pathological data. Images were interpreted independently and disagreements were resolved by discussion and consensus.

The following US characteristics were used to categorize each nodule: size; echogenicity; boundary; pattern of arterial phase enhancement; presence; timing; and degree of washout. The number of FLLs for each patient was also recorded.

The enhancement pattern of target lesions during the arterial phase were classified as follows: homogeneous hyperenhancement; heterogeneous hyperenhancement; peripheral rim-like hyperenhancement; isoenhancement; and hypoenhancement.[25] Washout time was calculated from the time of contrast agent injection to the time when the nodule began to show hypoenhancement compared with the surrounding hepatic parenchyma. Washout was classified as early when it occurred within 1 min from contrast injection. The washout, when occurring, was classified into mild and marked according to its degree by 2 min: a marked washout is defined as a punched-out appearance of the nodule. Based on qualitative CEUS features, the nodules were classified according to CEUS LI-RADS classification.[7]

Finally, digitized quantification of contrast enhancement was performed on the recorded video clip using the quantitative analysis software package VueBox®, Version 7.4 (Bracco, Italy). The analysis can display the mean, median and SD of intensity pixels within the ROI drawn on the image for each frame of the acquired sequence. In our study, the time-intensity curves were generated from a manually defined ROI, placed over the lesion and large enough to encompass as much of the lesion area as possible. A second ROI, serving as a potential internal reference, was drawn on the adjacent liver tissue at the same depth of the nodule, avoiding large blood vessels and cystic areas, for the necessary comparison upon which the enhancement patterns are defined. The analysis was carried out by the two same physicians with expertise in the use of VueBox®.

Respiratory movement artifacts were eliminated by automatic adjustments and, when necessary, by deleting selected frames in the post-processing analysis. Quantification was done on uncompressed linear data (raw data), which were linearly proportional to microbubble concentration. The results were expressed as intensity values after calculating the arithmetic mean of pixel intensities. A gamma variate fit was used as a statistical model to normalize the dispersion of gamma values in the perfusion analysis. Interobserver variability between two physicians was analyzed on a sample of 20 individuals from the derivation cohort. Further details regarding D-CEUS and quantification processes are reported in a position paper endorsed by the EFSUMB.[17,26]

Eight perfusion parameters were selected to characterize both blood volume and blood flow and were extracted from time-intensity curves: peak enhancement (PE, measured in arbitrary units [AU]); area under the wash-in curve (WiAUC, AU), wash-in rate (WiR, AU), rise time (RT, in s), time to peak (TTP, s), mean local transit time (MTT, s); area under the washout curve (WoAUC, AU), area under the wash-in and washout curve (WiWoAUC, AU).

To reduce intra- and interindividual perfusion variability, blood volume-related parameters (PE, WiR, WiAUC, WoAUC, and WiWoAUC) were expressed as a ratio between the lesion and surrounding liver parenchyma ([lesion parameter - surrounding parenchyma parameter]/surrounding parenchyma parameter). The entire quantification process, from drawing ROI to extrapolation of functional parameters, was performed by two authors (LG and MEA) and the mean values of the two measurements were considered for analysis.

All patients included in this study were divided into a prospective training cohort (n = 58), comprising patients from IRCCS Policlinico Universitario Agostino Gemelli (Rome), and a retrospective validation cohort (n = 30) comprising patients from both IRCCS Policlinico Universitario Agostino Gemelli (Rome) and IRCCS Azienda Ospedaliera - Universitaria di Bologna. The optimal logistic regression model was developed in the training cohort and confirmed in the validation cohort.

Statistical analyses

The demographic, clinical, US, and contrastographic variables of the enrolled patients were analyzed with univariable analysis using the following methods: t test, for continuous variables

Table 1. Baseline characteristics of the study population.

Baseline characteristics	Total (n = 58)	HCC (n = 32)	No HCC (n = 26)	*p* value
Male, n (%)	36 (62.1)	23 (71.9)	13 (50.0)	0.09
Female, n (%)	22 (37.9)	9 (28.1)	13 (50.0)	
Age (years), mean ± SD	67.3 ± 11.5	65.0 ± 11.8	69.2 ± 11.0	0.09
BMI (kg/m^2), median (IQR)	25.3 (23.4–30.0)	26.0 (23.5–30.0)	24.6 (23.1–30.5)	0.33
Etiology				
Alcohol use disorder	13 (22.4)	7 (21.9)	6 (23.1)	0.91
Autoimmune	1 (1.7)	0 (0.0)	1 (3.9)	0.45
HBV, n (%)	6 (10.3)	1 (3.1)	5 (19.2)	0.06
HCV, n (%)	15 (25.9)	13 (40.6)	2 (7.7)	**0.004**
Metabolic dysfunction-associated steatotic liver disease, n (%)	28 (48.3)	13 (40.6)	15 (57.7)	0.20
Laboratory				
Alpha-fetoprotein (ng/ml), median (IQR)	4.6 (2.7–70.0)	4.6 (3.0–62.0)	5.5 (2.0–235.0)	0.06
Carcinoembryonic antigen 19-9 (IU/ml), median (IQR)	33.7 (9.4–131.0)	8.7 (5.0–35.7)	84.0 (30.2–436.0)	0.07

Data were analyzed using: t test, for continuous variables (for equal or unequal variances, depending on whether the homoscedasticity assumption was met); χ^2 test, for nominal variables in presence of cells in the contingency table with counts >5; Fisher's exact test, for nominal variables in presence of at least one cell in the contingency table with a count ≤5. CEUS LI-RADS, contrast-enhanced ultrasound Liver Imaging Reporting and Data System; HCC, hepatocellular carcinoma.

(for equal or unequal variances, depending on whether the homoscedasticity assumption was met); χ^2 test, for dichotomous nominal variables in the presence of cells in the contingency table with counts >5; and Fisher's exact test, for dichotomous nominal variables in presence of at least one cell in the contingency table with a count ≤5. Variables that presented a probability below the Hosmer–Lemeshow cut-off (p <0.25) of verifying the null hypothesis of no association were considered for incorporation into the logistic regression model. The Wald test was used to determine the statistical significance of the predictive ability of adding a variable to the model. Given the number of expected outcome events (*i.e.* histopathological diagnosis of HCC), the derivation of a logistic regression model incorporating between three and five predictive variables was hypothesized.

The diagnostic accuracy of logistic regression models was evaluated by receiver operating characteristic (ROC) curve and relative AUC. The predicted probability threshold of the model for HCC diagnosis was determined by setting the specificity at 100% and maximizing the sensitivity. When evaluating performance at a given cut-off, sensitivity, specificity, PPV and negative predictive value (NPV) were computed.

Calibration of the models was assessed using the Hosmer–Lemeshow's good of fitness test. In accordance with Hosmer and Lemeshow simulations,[27] the test was carried out using as the number of group g both 10 and g = *no. predictor variables* + 1. Given the well-known limits of the good-of-fitness test (*i.e.* low power, and underestimation of overfitting), the model calibration was also evaluated using the calibration curve. The choice of the best model was carried out by comparison of full and reduced nested logistic regression models using the likelihood ratio test. Moreover, the choice of the best model was guided by model calibration and sensitivity. Table S1 shows the statistical analysis carried out to choose the optimal logistic regression model, in accordance with the research question. Statistical analysis was conducted using the statistical software Stata®, version SE18. The calibration curve was obtained using the Stata's *calibration belt* package.[28]

Results

Patient clinical data

According to the inclusion and exclusion criteria, 58 consecutive patients with liver lesions at risk but inconclusive for HCC were prospectively enrolled in the training group for this study (36 men and 22 women; 67.3 ± 11.5 years) to build a diagnostic model, whereas 30 patients were retrospectively enrolled for the validation of the model (25 men and 5 women; 72 ± 9.6 years). The detailed baseline characteristics of the patients, including age, sex, etiology of liver disease, and serum markers, are shown in Tables 1 and 2. Based on the histological examination, the selected nodules comprised 32

Table 2. Baseline characteristics of the validation cohort.

Characteristics	Total (n = 30)	HCC (n = 25)	No HCC (n = 5)	*p* value
Male, n (%)	25 (83.3)	22 (88.0)	3 (60.0)	0.18
Female, n (%)	5 (16.7)	3 (12.0)	2 (40.0)	
Age (years), mean ± SD	72.0 ± 9.6	71.6 ± 9.5	73.8 ± 11.1	0.33
CEUS LI-RADS classification				
LI-RADS 3, n (%)	6 (20.0)	5 (20.0)	1 (20.0)	0.84
LI-RADS 4, n (%)	7 (23.3)	6 (24.0)	1 (20.0)	
LI-RADS 5, n (%)	6 (20.0)	6 (24.0)	0 (0.0)	
LI-RADS M, n (%)	11 (36.7)	8 (32.0)	3 (60.0)	
Etiology				
Alcohol use disorder	7 (23.3)	6 (24.0)	1 (20.0)	0.67
Autoimmune	0 (0.0)	0 (0.0)	0 (0.0)	
HBV, n (%)	2 (6.7)	2 (8.0)	0 (0.0)	0.69
HCV, n (%)	9 (30.0)	7 (28.0)	2 (40.0)	0.48
Metabolic dysfunction-associated steatotic liver disease, n (%)	16 (53.3)	14 (56.0)	2 (40.0)	0.43

Data were analyzed using: t test, for continuous variables (for equal or unequal variances, depending on whether the homoscedasticity assumption was met); χ^2 test, for nominal variables in presence of cells in the contingency table with counts >5; Fisher's exact test, for nominal variables in presence of at least one cell in the contingency table with a count ≤5. CEUS LI-RADS: contrast-enhanced ultrasound Liver Imaging Reporting and Data System.

(55.2%) HCC, 15 (25.9%) ICC, and 11 (19.0%) liver metastasis in the training cohort and 25 (83.3%) HCC, 2 (6.7%) ICC, and three (10.0%) non-malignant lesions in the validation cohort.

There were no significant differences in clinical and pathological characteristics between HCC and non-HCC nodules except for the HCV etiology, which was more common in HCC group (p = 0.004).

US imaging characteristics

US features of both cohorts are shown in Tables 3 and 4. A statistically significant different distribution of basal US features between patients with and without HCC in the training cohort was present for number of nodules ≥4 (15.6% *vs*. 46.2%, p = 0.03) and irregular margins of the target lesion (15.6% *vs*. 46.2%, p = 0.01) (Table 3). A higher number of nodules was associated with a lower probability of HCC (adjusted odds ratio [aOR] 0.08; 95% CI 0.01–0.54).

In terms of CEUS, arterial phase enhancement was significantly different in the two groups of patients. Homogeneous hyperenhancement was more frequent in HCC (62.5% *vs*. 46.6%, p = 0.007), whereas peripheral rim-like hyperenhancement was more represented in non-HCC lesions (17.2% *vs*. 3.1%, p = 0.002).

In total, 46 of 58 (79%) nodules showed washout in the portal or late phase. The median washout time was 48.5 s in HCC (IQR 42.0–50.0 s) compared with 45.0 s in non-HCC lesions (IQR 37.0–50.0 s) (p = 0.10). Marked washout was found in 18.8% (6/32) of HCC lesions, in contrast to 26.9% (7/26) of non-HCC lesions (p = 0.68).

In the entire cohort, 45 patients (77.6%) were classified as LI-RADS M, five (8.6%) as LI-RADS 3, and eight (13.8%) as LI-RADS 4. Although almost all non-HCC malignancies were assigned to the LR-M category, 21 HCC (65.6%) were also classified as LR-M.

In terms of D-CEUS, two quantitative parameters related to lesion enhancement, PE and WiR, were significantly higher in patients with HCC (median PE ratio, 0.69 *vs*. 0.22 AU, p = 0.006; WiR ratio, median 2.66 *vs*. 1.18 AU, p = 0.002), whereas no significant differences were observed for time-related parameters reflecting both tumor wash-in (RT and TTP) and washout (MTT) (Table 3 and Fig. 1).

Finally, liver parenchyma stiffness values were high in both groups, consistent with fully developed cirrhosis, but were lower in patients with HCC compared with those without HCC; however, the difference did not reach statistical significance (35.4 *vs*. 49.6 kPa; p = 0.13) (Table 3).

Risk prediction model for HCC diagnosis

The optimal logistic regression model was identified incorporating the following predictive variables: sex (aOR 5.56; 95%

Table 3. Ultrasound imaging characteristic of the target focal liver lesions.

Characteristics	Total (n = 58)	HCC (n = 32)	No HCC (n = 26)	*p* value
Basal US characteristics				
Number of nodules, n (%)				
1	27 (46.6)	19 (59.4)	8 (30.8)	**0.03**
2	9 (15.5)	4 (12.5)	5 (19.2)	
3	5 (8.6)	4 (12.5)	1 (3.9)	
≥4	17 (29.3)	5 (15.6)	12 (46.2)	
Diameter (mm), median (IQR)	36.0 (24.0–56.0)	35.0 (20.5–45.0)	39.0 (25.0–60.0)	0.08
Irregular margins, n (%)	41 (70.7)	27 (84.4)	14 (53.9)	**0.01**
CEUS characteristics				
Enhancement, n (%) in the arterial phase				
Hypoenhancement	2 (3.5)	1 (3.1)	1 (3.9)	0.70
Isoenhancement	4 (6.9)	3 (9.4)	1 (3.9)	0.39
Homogeneous hyperenhancement	27 (46.6)	20 (62.5)	7 (26.9)	**0.007**
Heterogenous hyperenhancement	15 (25.9)	7 (21.9)	8 (30.8)	0.44
Rim-like hyperenhancement	10 (17.2)	1 (3.1)	9 (34.6)	**0.002**
Presence of washout	46 (79.3)	24 (75.0)	22 (84.6)	0.37
Marked washout	13 (22.4)	6 (18.8)	7 (26.9)	0.68
Washout time (s), median (IQR)	47.0 (40.0–50.0)	48.5 (42.0–50.0)	45.0 (37.0—50.0)	0.10
CEUS LI-RADS classification				
LI-RADS 3, n (%)	5 (8.6)	3 (9.4)	2 (7.7)	**0.01**
LI-RADS 4, n (%)	8 (13.8)	8 (25.0)	0 (0.0)	
LI-RADS M, n (%)	45 (77.6)	21 (65.6)	24 (92.3)	
D-CEUS characteristics, median (IQR)				
Peak enhancement ratio (AU)	0.4 (-0.2 to 1.6)	0.7 (0.0 to 1.9)	0.2 (-0.5 to 0.6)	**0.006**
WiAUC ratio (AU)	-0.3 (-0.5 to 9.2)	-0.2 (-0.5 to 0.5)	-0.3(-0.6 to 2.0)	0.33
WoAUC ratio (AU)	-0.2 (-0.5 to 0.6)	-0.1(-0.4 to 0.7)	-0.4(-0.6 to 0.2)	0.08
WiWoAUC ratio (AU)	-0.2 (-0.5 to 0.4)	-0.1 (-0.4 to 0.6)	-0.3 (-0.5 to 0.2)	0.12
WiR ratio (AU)	1.6 (0.4–4.3)	2.7 (1.3–7.9)	1.2 (0.2–1.6)	**0.002**
Rise time (s)	10.9 (8.0–14.5)	11.2 (8.7–13.4)	9.5 (7.3–15.5)	0.30
Time to peak (s)	12.8 (9.2–16.5)	12.8 (10.5–15.6)	13.1 (8.7–19.1)	0.15
Mean local transit time (s)	81.8 (47.3–134.7)	70.6 (49.3–117.7)	93.9 (46.6–321.8)	0.10
2D SWE				
Median (IQR) (kPa)	37.6 (24.1–51.8)	35.4 (23.6–48.1)	49.6 (24.6–58.2)	0.13

Data were analyzed using: t test, for continuous variables (for equal or unequal variances, depending on whether the homoscedasticity assumption was met); χ^2 test, for nominal variables in presence of cells in the contingency table with counts >5; Fisher's exact test, for nominal variables in presence of at least one cell in the contingency table with a count ≤5. 2D SWE, 2D shear-wave elastography; AU, arbitrary unit; CEUS, contrast-enhanced ultrasound; D-CEUS, dynamic contrast-enhanced ultrasound; HCC, hepatocellular carcinoma; LI RADS: Liver Imaging Reporting and Data System; WiAUC, area under the wash-in curve; WiR, wash-in rate; WiWoAUC, area under the wash-in and washout curve; WoAUC: area under the washout curve.

Table 4. Ultrasound imaging characteristic of the target focal liver lesions in the validation cohort.

Characteristics	Total (n = 30)	HCC (n = 25)	No HCC (n = 5)	*p* value
Basal ultrasound characteristics				
Number of nodules, n (%)				
1	24 (80.0)	19 (76.0)	5 (100.0)	0.75
2	4 (13.3)	4 (16.0)	0 (0.0)	
3	2 (6.7)	2 (8.0)	0 (0.0)	
≥4	0 (0.0)	0 (0.0)	0 (0.0)	
Diameter (mm), median (IQR)	21.0 (19.0–40.0)	21.0 (18.0–42.5)	21.0 (20.0–29.0)	0.31
CEUS characteristics				
Enhancement, n (%)				
Hypoenhancement	2 (6.7)	2 (8.0)	0 (0.0)	0.69
Isoenhancement	10 (33.3)	7 (28.0)	3 (60.0)	0.19
Homogeneous hyperenhancement	15 (50.0)	13 (52.0)	2 (40.0)	0.50
Heterogenous hyperenhancement	3 (10.0)	3 (12.0)	0 (0.0)	0.57
Rim-like hyperenhancement	0 (0.0)	0 (0.0)	0 (0.0)	
Washout	23 (76.7)	19 (76.0)	4 (80.0)	0.67
D-CEUS characteristics, median (IQR)				
Peak enhancement ratio (AU)	0.0 (-0.3 to 0.7)	0.1 (-0.3 to 0.7)	-0.1 (-0.3 to -0.1)	0.13
Wash-in rate ratio (AU)	0.3 (-0.1 to 1.1)	0.5 (-0.1 to 1.1)	-0.1 (-0.2 to 0.0)	0.28

CEUS and D-CEUS was performed on target lesions, defined as the lesions with the best ultrasound visualization. Data were analyzed using: t test, for continuous variables (for equal or unequal variances, depending on whether the homoscedasticity assumption was met); χ^2 test, for nominal variables in presence of cells in the contingency table with counts >5; Fisher's exact test, for nominal variables in presence of at least one cell in the contingency table with a count ≤5. AU, arbitrary unit; CEUS, contrast-enhanced ultrasound; D-CEUS, dynamic contrast-enhanced ultrasound; HCC, hepatocellular carcinoma.

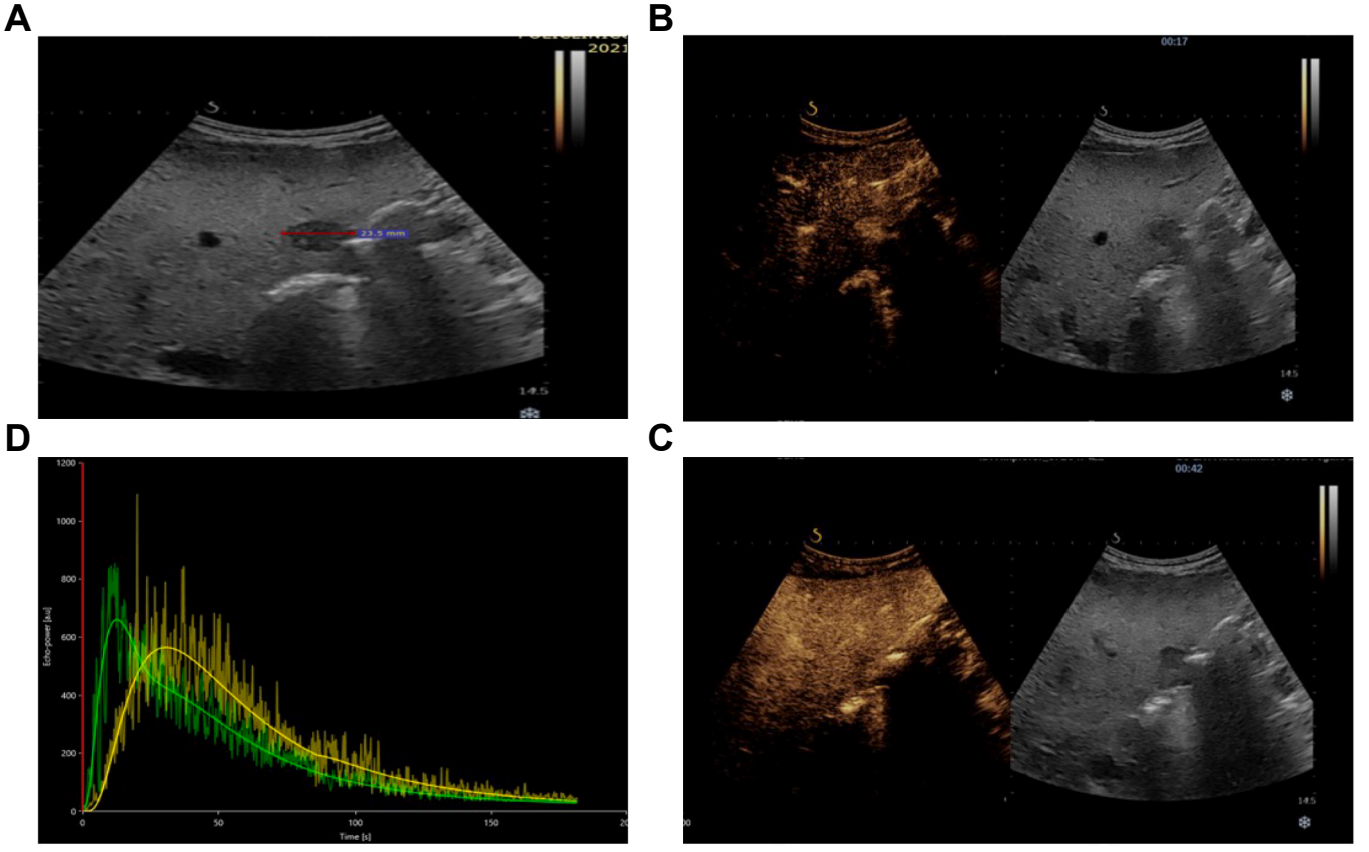

Fig. 1. US findings of a liver nodule diagnosed as HCC histopathologically. On CEUS examination, the nodule displayed heterogenous arterial phase hyperenhancement and portal venous phase early washout (time of washout was 42 s). According to CEUS LI-RADS, it was diagnosed as LR-M, whereas it was diagnosed as HCC by the PERSoN4 model (probability 79.8%). (A) B-mode showing a 23.5 mm hypo-echoic mass of the right liver lobe. (B) Arterial and (C) portal-venous phase CEUS images with corresponding time-intensity curve analysis (D) showing high PE and WiR. CEUS, contrast-enhanced ultrasound; HCC, hepatocellular carcinoma; LI-RADS, Liver Imaging Reporting and Data System; PERSoN4, Peak enhancement–Rim-like enhancement–Sex–Nodules≥4; PE, peak enhancement; US, ultrasound; WiR, wash-in rate.

CI: 1.19–25.94; p = 0.03), presence of four or more nodules (OR 0.08; 95% CI: 0.01–0.54; p = 0.01), presence of peripheral rim-like hyperenhancement (OR 0.08; 95% CI: 0.01-0.83; p = 0.03) and PE ratio (OR 2.51; 95% CI: 1.12–5.61; p = 0.03). β coefficients of the logistic regression model are reported in Table 5. According to the logistic regression model equation (Equation 1), the probability of HCC diagnosis [p(HCC)] was calculated using Equation 2 (probability of HCC diagnosis; p[HCC]).

$$\text{Ln(Odds)} = \text{Ln}[p(\text{HCC})/1\text{-}p(\text{HCC})] = -0.479 + 1.715^{a} - 2.484^{b} - 2.491^{c} + 0.919\times d \quad [1]$$

where a represents if male sex; b represents if ≥4 nodules; c represents if peripheral rim-like hyperenhancement present; and d represents the PE ratio.

$$p(\text{HCC}) = e^{\text{Lnp(HCC)}/1\text{-}p(\text{HCC})}/[1+ e^{\text{Lnp(HCC)}/1\text{-}p(\text{HCC})}] \quad [2]$$

Based on the ROC analysis, the PE–rim-like enhancement–sex–nodules≥4 (PERSoN4) logistic regression model showed high accuracy, with an AUC of 0.91 (95% CI: 0.83-0.98) (Fig. 2).

The predicted probability threshold of the model for HCC diagnosis was determined by setting the specificity at 100% and maximizing the sensitivity. The optimal cutoff value obtained by this approach was 0.7729 (Fig. 2). Hence, HCC diagnosis was defined as a score >0.7729 predicted by the PERSoN4 model. Applying this probability threshold, the model showed a sensitivity of 68.8% (95% CI: 50.0–83.9%) and a specificity of 100.0% (95% CI: 86.8–100.0%), with a PPV for HCC of 100.0% (95% CI: 83.2–100.0%) and moderate diagnostic accuracy (AUC 0.84, 95% CI: 0.76–0.93) (Fig. S1).

Moreover, the PERSoN4 logistic regression model demonstrated adequate calibration in both the Hosmer–Lemeshow's good of fitness test and calibration curve evaluation. In fact, according to the Hosmer–Lemeshow's good of fitness test, no evidence of lack of fitness was detected (p = 0.28, g = 5; p = 0.22, g = 10, respectively). According to the calibration curve, the PERSoN4 model was adequately fitted (p = 0.12), without significant evidence of underestimation or overestimation of HCC diagnosis in any segment of the expected/observed number of events function (Fig. S2).

An excellent level of interobserver agreement was observed. Using a two-way mixed-effects model for absolute agreement, estimated on a sample of 20 individuals from the derivation cohort, the intraclass correlation coefficient for single measures was 0.997 (95% CI: 0.991–0.999), showing minimal variability between readers. For the average of the two readers, the intraclass correlation coefficient was 0.998 (95% CI: 0.996–0.999). Both estimates were significantly greater than zero (p <0.001), confirming a very high degree of agreement between observers.

Table 5. Logistic regression model coefficients of the PERSoN4 model to predict HCC.

Predictive variable	β (95% CI)	p value
Male sex	1.715 (0.175–3.256)	0.03
Nodules ≥4	-2.484 (-4.346 to -0.623)	0.01
Peripheral rim-like hyperenhancement	-2.491 (-4.792 to -0.191)	0.03
Peak enhancement percentage change	0.919 (0.114–1.725)	0.03
Constant	-0.479 (-1.781 to 0.822)	N/A

HCC, hepatocellular carcinoma; PERSoN4, Peak enhancement–Rim-like enhancement–Sex–Nodules≥4.

A sensitivity analysis conducted on patients classified as LR-M with the CEUS LI-RADS algorithm (n = 45) showed similar accuracy and calibration. In this subgroup of patients, the PERSoN4 model had a sensitivity of 66.7% (95% CI: 43.0–85.4%) and a specificity of 100.0% (95 CI%: 85.8–100.0%), with an AUC of 0.83 (95% CI: 0.73–0.93) (Fig. S3). Furthermore, the Hosmer–Lemeshow's test (p = 0.18, g = 5; p = 0.11, g = 10) and the calibration curve (p = 0.12) showed no evidence of lack of fitness (Fig. S4).

On ROC analysis in the validation cohort, the PERSoN4 logistic regression model showed fair accuracy, with an AUC of 0.74 (95% CI: 0.53–0.96) (Fig. 2).

Applying the identified probability cutoff (score >0.7729), the model showed a sensitivity of 48.8% and a specificity of 100%, with a PPV for HCC of 100%. With this probability threshold, the model maintained a fair diagnostic accuracy, with an AUC of 0.74 (95% CI: 0.64–0.84) (Fig. S5).

The PERSoN4 logistic regression model also demonstrated adequate calibration in the validation cohort. According to the calibration curve, the model was adequately fitted (p = 0.40), without significant evidence of underestimation or overestimation of HCC diagnosis in any segment of the expected/observed number of events function (Fig. S6). Indeed, in this statistical test, a p value >0.05 supported the null hypothesis that the model was well calibrated, indicating that the predicted probabilities were consistent with the observed frequencies of HCC.

In Fig. 3, we provide a schematic illustrating the intended use of the PERSoN4 model.

Discussion

In the present study, we demonstrated that a multiparametric diagnostic model integrating clinical data with CEUS quantitative analysis achieved a level of diagnostic accuracy sufficient to allow a conclusive diagnosis of HCC in more than half of nodules classified as inconclusive by conventional CEUS LI-RADS criteria and otherwise referred for liver biopsy (*i.e.* LR3, LR4 and LR-M).

The improvement of non-invasive criteria for accurate diagnosis of FLLs is of widespread clinical interest especially in patients with chronic liver diasease.[29] Although LI-RADS emerges as a valuable diagnostic algorithm to support the management of liver tumors, many improvements are still needed to overcome current limitations. In fact, different studies and meta-analyses have shown that these criteria have only a moderate level of sensitivity in differentiating HCC from non-HCC malignanices.[30,31] In particular, the LR-M category provided a high NPV but low PPV for non-HCC malignancy diagnosis because of a high proportion of HCC misclassification.[14,15] Another proportion of HCC nodules are included in LR-3 and LR-4 categories, requiring the need of liver biopsies to correctly classify the lesions.

To increase the sensitivity of HCC detection and to reduce missed diagnoses, attempts have been made to improve the diagnostic accuracy of standard LI-RADS criteria. Previous studies focused mainly on the modification of imaging characteristics, such as adjusting the time to define early washout[15,32,33] or combining the time and degree of early washout,[16,34] but existing imaging techniques and tumor

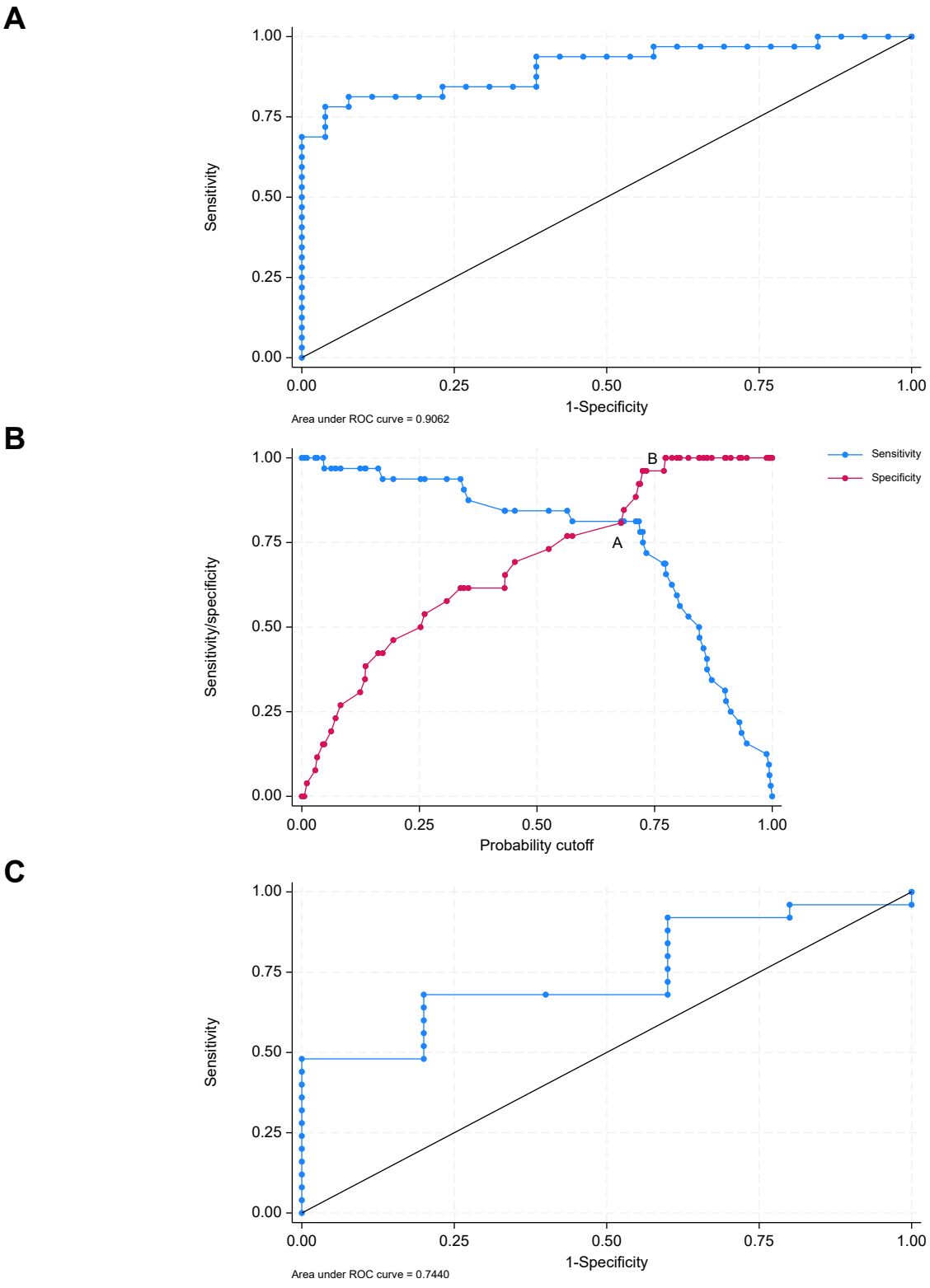

Fig. 2. Sensitivity and Specificity of the PERSoN4 model. (A) ROC analysis of the PERSoN4 logistic regression model. (B) Sensitivity and specificity of the PERSoN4 model with respect to the predicted probability of HCC. (A) Youden's Index = 0.7192. (B) PERSoN4 model threshold = 0.7729. (C) ROC analysis of the PERSoN4 logistic regression model in the validation cohort. HCC, hepatocellular carcinoma; PE: Peak Enhancement; PERSoN4: Peak enhancement–Rim-like enhancement–-Sex-Nodules≥4; ROC, receiver operating characteristics.

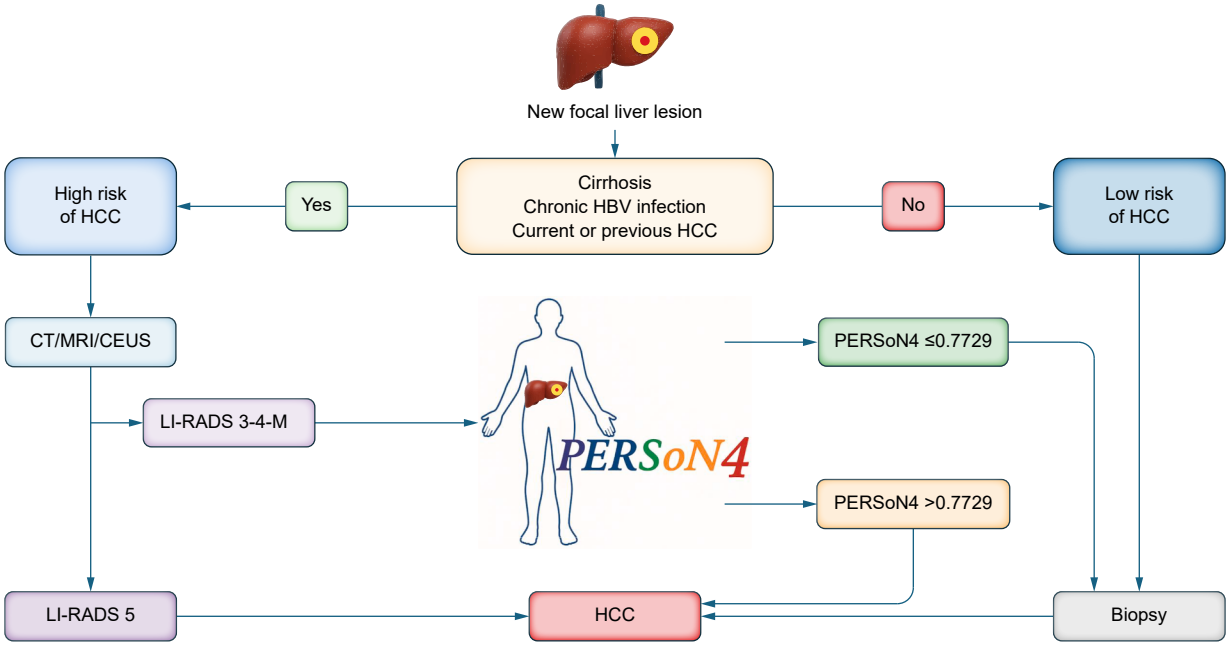

Fig. 3. Proposed algorithm for the use of the PERSoN4 model. HCC, hepatocellular carcinoma; PE, peak enhancement; PERSoN4, Peak enhancement–Rim-like enhancement–Sex–Nodules≥4.

biomarkers remain insufficient to correctly differentiate HCC from other liver malignancies.

The role of imaging in the multidisciplinary approach of patients with HCC is constantly evolving and expanding because of the application of newer quantitative techniques that evaluate blood perfusion. In particular, the quantification of CEUS signals has been used to complement the qualitative assessment of FLLs, showing significant differences not only between benign and malignant lesions,[35] but also in predicting tumor biological behavior. This type of analysis, also termed D-CEUS, can detect more marked washout in cholangiocarcinoma than in HCC[36] and microvascular invasion of HCC, based on parameters such as wash-in rate and washout rate.[37] Therefore, we used D-CEUS features to improve the diagnostic accuracy of standard LI-RADS criteria.

In this cohort study, we developed and evaluated the diagnostic performance of a new multiparametric score based on D-CEUS parameters for the non-invasive diagnosis of HCC in high-risk patients with inconclusive previous imaging (CT/MRI and CEUS). Our results demonstrated that, by adding quantitative and clinical parameters to CEUS observations, the PERSoN4 logistic regression model could be a useful tool for HCC diagnosis (AUC 0.91; 95% CI: 0.83–0.98). Given that the primary purpose of our study was to provide high specificity for the diagnosis of HCC, the predicted probability threshold of the model was determined by setting the specificity at 100% and maximizing the sensitivity. The derived probability threshold (0.7729) allowed a non-invasive diagnosis of HCC in 68.8% of patients eligible for liver biopsy, with good accuracy (AUC 0.83; 95% CI: 0.76–0.93).

Interestingly, AFP showed a nonsignificant association with HCC. However, given a p value of <0.25, we attempted to include AFP in the model, but it did not improve its discriminative performance. This might be explained by the exclusion of CEUS LI-RADS LR-5 lesions, which typically exhibit higher AFP levels, in contrast to atypical HCC cases.

Although our results were not perfect, the high AUC, sensitivity, and specificity of the PERSoN4 model indicated promising discrimination ability and accuracy. As a result, earlier and more confident diagnosis of HCC could be achieved. This might be helpful in clinical practice to avoid the use of percutaneous biopsies, which can cause bleeding or implantation metastasis,[38] at least in a subgroup of patients.

It is already known that CEUS enables the possibility of real-time assessment of arterial phase enhancement, which might be missed or misinterpreted in other imaging studies. The peculiarity of CEUS in intercepting arterial phase enhancement is reflected positively not only in the downgrade of LR-3 or LR-4 formations, but also in the definitive diagnosis of HCC.[39]

D-CEUS can improve the diagnostic accuracy of visual interpretation because it enables characterization of the nodule microperfusion relative to the adjacent liver tissue in a more comprehensive and reproducible manner.[40,41]

However, previous studies focused on using D-CEUS to evaluate the nodule washout time more objectively and accurately and to improve the diagnostic performance of LR-5 for HCC.[20,42] By contrast, our study underlined the role of PE and combined clinical and multiparametric imaging data to explore and improve a non-invasive diagnostic algorithm for HCC in high-risk patients.

We previously demonstrated that CEUS parameters combined with stiffness values and liver background could be useful for the differential diagnosis between HCC and ICC in the general population.[21] The present study extends the analysis of individual CEUS features to a predictive model-based differential diagnostic approach combining imaging and clinical data in a different population. However, in this case, we focused on high-risk patients to optimize as much as possible the non-invasive diagnosis of HCC, with promising results. This approach would allow a non-invasive diagnosis of HCC in nearly 70% of nodules not classified with traditional imaging criteria. Furthermore the PERSoN4 model is not intended to

replace CEUS LI-RADS but to be applied sequentially in those cases classified as LR-3, LR-4, or LR-M, where the CEUS LI-RADS assessment remains inconclusive (Fig. 3).

These characteristics make it a promising model, which maintained expectations when validated on an external cohort. The PERSoN4 model presents considerable sensitivity and adequate calibration. In fact, the derivation cohort showed a sensitivity of 68.8%, whereas, in the validation cohort, a sensitivity of 48.8% was documented. This would enable non-invasive diagnosis of HCC in almost one out of two patients with cirrhosis currently referred for liver biopsy.

The model maintained good diagnostic accuracy despite the validation cohort presenting a low prevalence of ICC and liver metastasis. Indeed, in the validation cohort, there were no patients with rim enhancement or with four or more nodules. This makes the model even more promising when applied in the context of a more heterogeneous cohort. If these findings are confirmed in larger population and in different cohorts, our predictive model could become a useful tool in clinical practice.

The present study has some limitations. First, only a small number of patients were enrolled. However, the number of patients referred for biopsy after inconclusive contrast imaging study is not high and this limited the collection of the training cohort, whereas the availability of a sufficiently long adequate CEUS video clip of patients with histological diagnosis limited the collection of the retrospective validation group. Thus, a multicenter cohort study with larger sample size is needed to validate this RPM. Second, according to the recommendations of the CEUS LI-RADS system,[7] we enrolled only patients at high risk for HCC, and we did not evaluate the performance of the model in patients without cirrhotic background. However, in our cohort, and contrary to previous work,[15] the incidence of HCC and non-HCC malignancies was comparable, with most falling in the LR-M class. This is an important strength that could influence the reliability of the results and the possibility to extend the model to other subgroups of patient after appropriate validation. Third, US is an operator-dependent technique with lower sensitivity in patients with obesity and patients with abdominal bloating; thus, not all potential nodules might be adequately evaluated with this non-invasive imaging modality. Moreover, there are technical limitations of D-CEUS. The decision to include as much of the tumor area as possible inside the ROI could lead to more heterogeneity. Another issue is the individual situation of liver perfusion, which limits interindividual comparability of D-CEUS values. To achieve greater comparability, D-CEUS parameters of liver lesions were 'normalized' according to the enhancement of the nearby liver parenchyma. Finally, the acquisition of D-CEUS clips and time-intensity-curves as well as the whole analysis of parametric imaging are not easy to apply; thus, the feasibility and usefulness of the method in clinical practice remain challenging.

Despite these limitations, the PERSoN4 model appears to be a valuable tool for the non-invasive diagnosis of HCC in patients with cirrhosis currently referred for liver biopsy. The high diagnostic accuracy and good calibration of approach make it a promising model, which maintained expectations when validated on an external cohort.

Concluding remarks

The D-CEUS-based PERSoN4 risk assessment model appears to be a valuable tool for the dynamic assessment of nodule microvascularization and could enhance the performance of the standard CEUS LI-RADS algorithm for the non-invasive diagnosis of HCC in high-risk patients with inconclusive findings. In our cohort, this diagnostic model allowed for the non-invasive diagnosis of HCC at least in half of patients who are currently candidates to liver biopsy, with a PPV of 100%. However, multicenter cohorts with large study groups are required to evaluate the reproducibility and applicability of these findings in different populations and clinical settings.

Affiliations

[1]*CEMAD Digestive Disease Center, Fondazione Policlinico Universitario "A. Gemelli" IRCCS, Università Cattolica del Sacro Cuore di Roma, Rome, Italy;* [2]*Thrombosis Unit, Fondazione Policlinico Universitario "A. Gemelli" IRCCS, Università Cattolica del Sacro Cuore di Roma, Rome, Italy;* [3]*Division of Internal Medicine, Hepatobiliary and Immunoallergic Diseases, IRCCS Azienda Ospedaliero-Universitaria di Bologna, Italy*

Abbreviations

2D SWE, 2D shear-wave elastography; ACR, American College of Radiology; AFP, alpha-fetoprotein; aOR, adjusted odds ratio; AU, arbitrary unit; CA 19-9, carcinoembryonic antigen 19-9; CEUS, contrast-enhanced ultrasound; D-CEUS, dynamic contrast-enhanced ultrasound; DICOM, Digital Imaging and Communications in Medicine; EFSUMB, European Federation for Ultrasound in Medicine and Biology; FLL, focal liver lesion; HCC, hepatocellular carcinoma; ICC, intrahepatic cholangiocellular carcinoma; LI-RADS, Liver Imaging Reporting and Data System; MTT, mean local transit time; NPV, negative predictive value; OR, odds ratio; PE, peak enhancement; PERSoN4, Peak enhancement–Rim-like enhancement–Sex–Nodules≥4; PPV, positive predictive value; ROC, receiver operating characteristics; ROI, region of interest; RPM, risk prediction model; RT, rise time; SI, stability index; TTP, time to peak; US, ultrasound; WiAUC, area under the wash-in curve; WiR, wash-in rate; WiWoAUC, area under the wash-in and washout curve; WoAUC, area under the washout curve.

Financial support

This research received no external funding.

Conflict of interest

The authors have no conflict of interest to declare.

Please refer to the accompanying ICMJE disclosure forms for further details.

Authors' contributions

Conceptualization: MAZ. Data curation: PS. Formal analysis: PS, LG. Investigation: MAZ, MEA, LR, MG, GE, IM, MP, RB, AG. Methodology: MAZ, MEA. Project administration: MAZ. Resources: MAZ, LR, LC, MP, FP. Software: PS. Supervision: MP, AG. Writing – original draft: PS, MEA. Writing – review & editing: MAZ, FP.

Data availability

All data generated or analyzed during this study are included in this article and its supplementary material files. Further enquiries should be directed to the corresponding author.

Acknowledgements

We thank Fondazione Roma for their continuous support of our scientific research.

Supplementary data

Supplementary data to this article can be found online at https://doi.org/10.1016/j.jhepr.2026.101823.

References

Author names in bold designate shared cofirst authorship

[1] **Claudon M**, **Dietrich CF**, Choi BI, et al. Guidelines and good clinical practice recommendations for contrast enhanced ultrasound (CEUS) in the liver - update 2012. Ultraschall Med 2013;34:11–29.

[2] Schellhaas B, Bernatik T, Dirks K, et al. Contrast-enhanced ultrasound patterns for the non-invasive diagnosis of hepatocellular carcinoma: a prospective multicenter study in histologically proven liver lesions in a real-life setting demonstrating the benefit of extended late phase observation. Ultrasound Med Biol 2021;47:3170–3180.

[3] Zhou J, Sun HC, Wang Z, et al. Guidelines for diagnosis and treatment of primary liver cancer in China (2017 edition). Liver Cancer 2018;7:235–260.

[4] European Association for the Study of the Liver. EASL Clinical Practice Guidelines on the management of hepatocellular carcinoma. J Hepatol 2025;82:315–374.

[5] Kudo M. Surveillance, diagnosis, and treatment outcome of hepatocellular carcinoma in Japan: 2023 update. Liver Cancer 2023;12:95–102.

[6] Vogel A, Cervantes A, Chau I, et al. Hepatocellular carcinoma: ESMO Clinical Practice Guidelines for diagnosis, treatment and follow-up. Ann Oncol 2018;29:iv238–iv255.

[7] Kono Y, Lyshchik A, Cosgrove D, et al. Contrast enhanced ultrasound (CEUS) liver imaging reporting and data system (LI-RADS®): the official version by the American College of Radiology (ACR). Ultraschall Med 2017;38:85–86.

[8] Ding J, Long L, Zhou H, et al. The predictive value of Liver Imaging Reporting and Data System with contrast-enhanced ultrasound (v2017) in the risk of hepatocellular carcinoma in high-risk population. Chin J Ultrason 2020;29:138–142.

[9] Wilson SR, Lyshchik A, Piscaglia F, et al. CEUS LI-RADS: algorithm, implementation, and key differences from CT/MRI. Abdom Radiol 2018;43:127–142.

[10] Huang JY, Li JW, Lu Q, et al. Diagnostic accuracy of CEUS LI-RADS for the characterization of liver nodules 20 mm or smaller in patients at risk for hepatocellular carcinoma. Radiology 2020;294:329–339.

[11] Terzi E, Iavarone M, Pompili M, et al. Contrast ultrasound LI-RADS LR-5 identifies hepatocellular carcinoma in cirrhosis in a multicenter retrospective study of 1,006 nodules. J Hepatol 2018;68:485–492.

[12] Lyshchik A, Kuon Yeng Escalante C, Xiao TS, et al., Trial Group, CEUS LI-RADS Trial Group Members. Contrast-enhanced US of high-risk indeterminate focal liver observations categorized as LR-4 or LR-M at CT/MRI. Radiology 2025 Jan;314:e240916.

[13] Zhou H, Zhang C, Du L, et al. Contrast-enhanced ultrasound liver imaging reporting and data system in diagnosing hepatocellular carcinoma: diagnostic performance and interobserver agreement. Ultraschall Med 2022;43:64–71.

[14] Chen L Da, Ruan SM, Lin Y, et al. Comparison between M-score and LR-M in the reporting system of contrast-enhanced ultrasound LI-RADS. Eur Radiol 2019;29:4249–4257.

[15] Ding J, Qin Z, Zhou Y, et al. Impact of revision of the LR-M criteria on the diagnostic performance of contrast-enhanced ultrasound LI-RADS. Ultrasound Med Biol 2021;47:3403–3410.

[16] Zeng D, Xu M, Liang JY, et al. Using new criteria to improve the differentiation between HCC and non-HCC malignancies: clinical practice and discussion in CEUS LI-RADS 2017. Radiol Med 2022;127:1–10.

[17] Dietrich CF, Correas JM, Cui XW, et al. EFSUMB Technical Review - update 2023: dynamic contrast-enhanced ultrasound (DCE-CEUS) for the quantification of tumor perfusion. Ultraschall Med 2024;45:36–46.

[18] Li R, Zhang X, Ma KS, et al. Dynamic enhancing vascular pattern of intrahepatic peripheral cholangiocarcinoma on contrast-enhanced ultrasound: the influence of chronic hepatitis and cirrhosis. Abdom Imag 2013;38:112–119.

[19] Anaye A, Perrenoud G, Rognin N, et al. Differentiation of focal liver lesions: usefulness of parametric imaging with contrast-enhanced US. Radiology 2011;261:300–310.

[20] Qiu S, Ding J, Qin Z, et al. Application of DCE-US using the LI-RADS for patients with liver nodules at high risk for hepatocellular carcinoma: a preliminary study and comparison with visual interpretation. Eur J Radiol 2022;155:110473.

[21] Ainora ME, Cerrito L, Liguori A, et al. Multiparametric dynamic ultrasound approach for differential diagnosis of primary liver tumors. Int J Mol Sci 2023;24:8548.

[22] Wildner D, Schellhaas B, Strack D, et al. Differentiation of malignant liver tumors by software-based perfusion quantification with dynamic contrast-enhanced ultrasound (DCEUS). Clin Hemorheol Microcirc 2019;71:39–51.

[23] Wildner D, Pfeifer L, Goertz RS, et al. Dynamic contrast-enhanced ultrasound (DCE-US) for the characterization of hepatocellular carcinoma and cholangiocellular carcinoma. Ultraschall Med 2014 Dec;35:522–527.

[24] Lurie Y, Webb M, Cytter-Kuint R, et al. Non-invasive diagnosis of liver fibrosis and cirrhosis. World J Gastroenterol 2015;21:11567–11583.

[25] Chen L Da, Ruan SM, Liang JY, et al. Differentiation of intrahepatic cholangiocarcinoma from hepatocellular carcinoma in high-risk patients: a predictive model using contrast-enhanced ultrasound. World J Gastroenterol 2018;24:3786–3798.

[26] Dietrich CF, Averkiou MA, Correas JM, et al. An EFSUMB introduction into dynamic contrast-enhanced ultrasound (DCE-US) for quantification of tumour perfusion. Ultraschall Med 2012;33:344–351.

[27] Hosmer Jr DW, Lemeshow S, Sturdivant RX. Applied logistic regression. 3rd ed. Hoboken: John Wiley & Sons; 1989.

[28] Nattino G, Finazzi S, Bertolini G. A new calibration test and a reappraisal of the calibration belt for the assessment of prediction models based on dichotomous outcomes. Stat Med 2014;33:2390–2407.

[29] Seitz K, Greis C, Schuler A, et al. Frequency of tumor entities among liver tumors of unclear etiology initially detected by sonography in the non-cirrhotic or cirrhotic livers of 1349 patients. Results of the DEGUM multicenter study. Ultraschall Med 2011;32:598–603.

[30] Son JH, Choi SH, Kim SY, et al. Accuracy of contrast-enhanced ultrasound liver imaging reporting and data system: a systematic review and meta-analysis. Hepatol Int 2020;14:1104–1113.

[31] Shin J, Lee S, Bae H, et al. Contrast-enhanced ultrasound liver imaging reporting and data system for diagnosing hepatocellular carcinoma: a meta-analysis. Liver Int 2020;40:2345–2352.

[32] Li F, Li Q, Liu Y, et al. Distinguishing intrahepatic cholangiocarcinoma from hepatocellular carcinoma in patients with and without risks: the evaluation of the LR-M criteria of contrast-enhanced ultrasound liver imaging reporting and data system version 2017. Eur Radiol 2020;30:461–470.

[33] Huang W, Wen R, Wu Y, et al. Can modifications of LR-M Criteria improve the diagnostic performance of contrast-enhanced ultrasound LI-RADS for small hepatic lesions up to 3 cm? J Ultrasound Med 2023;42:2403–2413.

[34] Zheng W, Li Q, Zou XB, et al. Evaluation of contrast-enhanced US LI-RADS version 2017: application on 2020 liver nodules in patients with hepatitis B infection. Radiology 2020;294:299–307.

[35] Schwarz S, Clevert DA, Ingrisch M, et al. Quantitative analysis of the time-intensity curve of contrast-enhanced ultrasound of the liver: differentiation of benign and malignant liver lesions. Diagnostics 2021;11:1244.

[36] Wildner D, Pfeifer L, Goertz RS, et al. Dynamic contrast-enhanced ultrasound (DCE-US) for the characterization of hepatocellular carcinoma and cholangiocellular carcinoma. Ultraschall Med 2014;35:522–527.

[37] Dong Y, Qiu Y, Yang D, et al. Potential application of dynamic contrast enhanced ultrasound in predicting microvascular invasion of hepatocellular carcinoma. Clin Hemorheol Microcirc 2021;77:461–469.

[38] Kleiner DE. Hepatocellular carcinoma: liver biopsy in the balance. Hepatology 2018;68:13–15.

[39] Bartolotta TV, Terranova MC, Gagliardo C, et al. CEUS LI-RADS: a pictorial review. Insights Imaging 2020;11:9.

[40] Dietrich CF, Nolsøe CP, Barr RG, et al. Guidelines and good clinical practice recommendations for contrast-enhanced ultrasound (CEUS) in the Liver-Update 2020 WFUMB in Cooperation with EFSUMB, AFSUMB, AIUM, and FLAUS. Ultrasound Med Biol 2020;46:2579–2604.

[41] Pei XQ, Liu LZ, Liu M, et al. Contrast-enhanced ultrasonography of hepatocellular carcinoma: correlation between quantitative parameters and histological grading. Br J Radiol 2012;85:e740–e747.

[42] Wildner D, Schellhaas B, Strack D, et al. Differentiation of malignant liver tumors by software-based perfusion quantification with dynamic contrast-enhanced ultrasound (DCEUS). Clin Hemorheol Microcirc 2019;71:39–51.

Keywords: DCE-US; HCC; CEUS LI-RADS.
Received 30 August 2025; received in revised form 4 March 2026; accepted 6 March 2026; Available online 12 March 2026